Selectivity of plasma membrane calcium ATPase (PMCA)-mediated extrusion of toxic divalent cations in vitro and in cultured cells

Mariela S. Ferreira-Gomes, Irene C. Mangialavori, Mallku Q. Ontiveros, Debora E. Rinaldi, Jorge Martiarena, Sandra V. Verstraeten, et al.

Archives of Toxicology

ISSN 0340-5761

Arch Toxicol
DOI 10.1007/s00204-017-2031-9

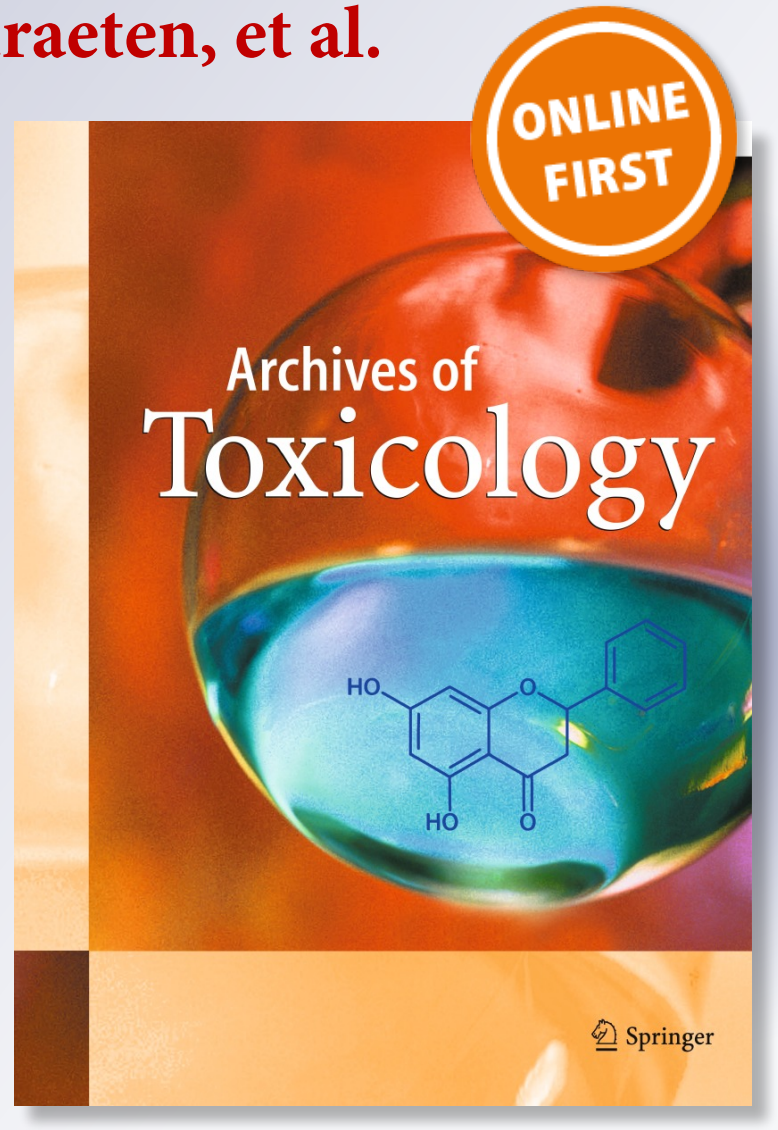

Springer

Arch Toxicol
DOI 10.1007/s00204-017-2031-9

MOLECULAR TOXICOLOGY

Selectivity of plasma membrane calcium ATPase (PMCA)-mediated extrusion of toxic divalent cations in vitro and in cultured cells

Mariela S. Ferreira-Gomes[1] · Irene C. Mangialavori[1] · Mallku Q. Ontiveros[1] · Debora E. Rinaldi[1] · Jorge Martiarena[1] · Sandra V. Verstraeten[1] · Juan Pablo F. C. Rossi[1]

Received: 17 April 2017 / Accepted: 12 July 2017

Abstract In the recent years, the toxicity of certain divalent cations has been associated with the alteration of intracellular Ca^{2+} homeostasis. Among other mechanisms, these cations may affect the functionality of certain Ca^{2+}-binding proteins and/or Ca^{2+} pumps. The plasma membrane calcium pump (PMCA) maintains Ca^{2+} homeostasis in eukaryotic cells by mediating the efflux of this cation in a process coupled to ATP hydrolysis. The aim of this work was to investigate both in vitro and in cultured cells if other divalent cations (Sr^{2+}, Ba^{2+}, Co^{2+}, Cd^{2+}, Pb^{2+} or Be^{2+}) could be transported by PMCA. Current results indicate that both purified and intact cell PMCA transported Sr^{2+} with kinetic parameters close to those of Ca^{2+} transport. The transport of Pb^{2+} and Co^{2+} by purified PMCA was, respectively, 50 and 75% lower than that of Ca^{2+}, but only Co^{2+} was extruded by intact cells and to a very low extent. In contrast, purified PMCA—but not intact cell PMCA—transported Ba^{2+} at low rates and only when activated by limited proteolysis or by phosphatidylserine addition. Finally, purified PMCA did not transport Cd^{2+} or Be^{2+}, although minor Be^{2+} transport was measured in intact cells. Moreover, Cd^{2+} impaired the transport of Ca^{2+} through various mechanisms, suggesting that PMCA may be a potential target of Cd^{2+}-mediated toxicity. The differential capacity of PMCA to transport these divalent cations may have a key role in their detoxification, limiting their noxious effects on cell homeostasis.

Keywords Divalent cation toxicity · Plasma membrane calcium pump · Ion transport · Calcium homeostasis

Abbreviations

[^{125}I]TID-PC/16	1-*O*-hexadecanoyl-2-*O*-[9-[[[2-[^{125}I]iodo-4-(trifluoromethyl-3H-diazirin-3-yl)benzyl]oxy]carbonyl] nonanoyl]-*sn*-glycero-3-phosphocholine
$C_{12}E_{10}$	Polyoxyethylene 10 lauryl ether
CaM	Calmodulin
DC	Divalent cation
DMPC	Dimyristoyl phosphatidylcholine
DMSO	Dimethylsulfoxide
DTT	Dithiothreitol
EGTA	Ethylene glycol tetraacetic acid
eIOVs	Erythrocyte inside-out vesicles
ER	Endoplasmic reticulum
MOPS	3-(*N*-morpholino)propanesulfonic acid
PC	Phosphatidylcholine
PMCA	Plasma membrane calcium pump
PS	Phosphatidylserine
RB	Reaction buffer
SERCA	Sarco(endo)plasmic reticulum Ca^{2+}-ATPase
SOCs	Store-operated calcium channels
TG	Thapsigargin
TLCK	*N*-α-tosyl-L-lysine chloromethyl ketone

Mariela S. Ferreira-Gomes and Irene C. Mangialavori contributed equally to this work.

Electronic supplementary material The online version of this article (doi:10.1007/s00204-017-2031-9) contains supplementary material, which is available to authorized users.

✉ Sandra V. Verstraeten
verstraeten@ffyb.uba.ar

✉ Juan Pablo F. C. Rossi
jprossi@qb.ffyb.uba.ar

[1] Universidad de Buenos Aires, Consejo Nacional de Investigaciones Científicas y Técnicas (CONICET), Instituto de Química y Fisicoquímica Biológicas (IQUIFIB), Facultad de Farmacia y Bioquímica, Junín 956, Ciudad Autónoma de Buenos Aires C1113AAD, Argentina

Published online: 18 July 2017

Introduction

Plasma membrane calcium pump (PMCA) is a P-type ATPase involved in the maintenance and regulation of the low steady-state concentrations of Ca^{2+} in the cytoplasm of all eukaryotic cells. In humans, there are four genes that code for PMCA isoforms 1–4, and the alternative splicing of the mRNA regions coding for the two regulatory domains adds more isoform diversity. While PMCA1 and PMCA4 are ubiquitously distributed among tissues, PMCA2 and PMCA3 show a more restricted expression pattern, predominating in excitable cells (Strehler and Zacharias 2001). Erythrocyte membranes are enriched in PMCA4, the most regulated PMCA isoform. Since the binding site and the regions involved in Ca^{2+} transport are highly conserved among the different PMCA isoforms, the results obtained in this work using purified erythrocyte PMCA could be extrapolated to the behavior expected for PMCAs from other cells.

PMCA couples the efflux of Ca^{2+} to the hydrolysis of ATP to ADP and inorganic phosphate. The current kinetic model for PMCA activity proposes that the enzyme passes through different reaction intermediaries during the transport of Ca^{2+}. Cytoplasmic Ca^{2+} binds to the E_1 conformation of PMCA that, upon phosphorylation, generates the intermediate E_1P. After a conformational transition toward E_2P, Ca^{2+} is released to the extracellular milieu and the phosphoenzyme is hydrolyzed. This conformation (E_2) suffers a new transition to regenerate E_1, thus completing the cycle (Ferreira-Gomes et al. 2011; Rega and Garrahan 1986).

Several modulators regulate the activity of PMCA (Lopreiato et al. 2014). When the intracellular concentration of Ca^{2+} rises, it binds to calmodulin (CaM) and this complex interacts with the auto-inhibitory domain of PMCA located at the C-terminal region. In consequence, the pump undergoes a large conformational change from an inhibited state to an activated one (Mangialavori et al. 2009). Further accumulation of Ca^{2+} activates the protease calpain which causes partial proteolysis of PMCA in a site that is located upstream of the CaM-binding domain (Silbergeld 1992). As a result, PMCA becomes constitutively activated and insensitive to further modulation by CaM (James et al. 1989). Similarly, the interaction of acidic phospholipids [phosphatidylserine (PS) and phosphatidylinositol 3,4-bisphosphate] with the cytoplasmic domain of PMCA increases its apparent affinity for Ca^{2+}, allowing the pump to reach its maximal activity (Filoteo et al. 1992).

Certain divalent cations (DCs), such as cadmium (Cd^{2+}) and lead (Pb^{2+}), have no biological functions and are extremely cytotoxic (Verstraeten 2014), even at low concentrations. These DCs disrupt the homeostasis of Ca^{2+} (Simons 1993; Thevenod and Lee 2013), possibly by interfering with the functioning of certain Ca^{2+}-binding proteins, including PMCA. In this regard, it has been reported that PMCA is capable of transporting other metal cations besides Ca^{2+}, provided they are divalent and have ionic radii close to that of Ca^{2+} (Pfleger and Wolf 1975). However, it is still unclear whether toxic DCs may affect the transporting and/or ATPase activities of PMCA that could account for the disturbance of Ca^{2+} homeostasis observed in DCs-exposed tissues.

On this basis, we hypothesized that one of the mechanisms underlying strontium (Sr^{2+}), barium (Ba^{2+}), cobalt (Co^{2+}), Cd^{2+}, Pb^{2+} and beryllium (Be^{2+}) toxicity may be the alteration of normal PMCA activity that results in their accumulation in the cytoplasm. These DCs were selected based on the similitude of their ionic radii with that of Ca^{2+} and on the fact that most of them were reported to disturb Ca^{2+} homeostasis. Despite being a DC, Be^{2+} has smaller ionic radius and, therefore, it may establish different kinds of interactions with amino acids at the PMCA access channel. For this reason, minimal transport of Be^{2+} by PMCA can be expected. To verify this hypothesis, experiments were performed both in cultured human embryonic kidney (HEK293T) cells and in erythrocyte plasma membrane inside-out vesicles (eIOVs).

Overall, this study suggests that DCs entry in intact HEK293T cells occurs mostly through the store-operated Ca^{2+} channels (SOCs), although they have different capacities to exit cells via PMCA. In addition, it provides biochemical evidence of the consequences of Sr^{2+}, Ba^{2+}, Co^{2+}, Cd^{2+}, Pb^{2+} and Be^{2+} with PMCA, focusing on the capability of PMCA immersed in its native membrane environment to transport the DCs, on the promotion of the proper PMCA conformational changes required for DC transport, and on the effects of the DCs on PMCA ATPase activity. Furthermore, we characterized the interaction of the DCs with the main regulator of PMCAs, CaM. Altogether, current findings provide insights about the mechanisms underlying PMCA transport of diverse DCs and the possibility that this pump may be involved in DC cell detoxification is discussed.

Materials and methods

Reagents and biological samples

Human embryonic kidney (HEK293T) cells were obtained from American Type Culture Collection (ATCC, Manassas, VA). Dulbecco's modified Eagle's medium (DMEM), fetal bovine serum (FBS) and cell culture supplements were from Invitrogen (Carlsbad, CA, USA). The fluorescent probes Fura-2-AM and calcein-AM were purchased from Molecular Probes (Eugene, OR, USA). ^{125}I was obtained from Perkin-Elmer NEN Life Sciences Inc. (Boston, MA, USA). Calmodulin (CaM) was obtained from Calbiochem (La Jolla, CA, USA). Dimyristoyl phosphatidylcholine (PC)

was from Avanti Lipids (Alabaster, AL, USA). Phosphatidylserine (PS) from bovine brain, thapsigargin (TG) and all the other chemicals used in this work were of analytical grade and were purchased from Sigma-Aldrich (St. Louis, MO, USA). Freshly drawn human blood for the isolation of PMCA was obtained from Fundación Fundosol (Buenos Aires, Argentina). Donors provided informed consent for the donation of blood and for its subsequent legitimate use by the transfusion service. The DCs were incorporated to the reaction medium as $CaCl_2$, $BaCl_2$, $SrCl_2$, $Pb(NO_3)_2$, $CoCl_2$, $CdCl_2$ and $BeSO_4$. Before their use, residual Ca^{2+} and/or other DCs were removed from buffers and solutions before their use using a Chelex-100 column (Liu et al. 1997).

Cell culture

HEK293T cells were cultured in DMEM supplemented with 10% (v/v) FBS and 1% (v/v) antibiotic/antimycotic solution (Life Technologies Inc., Carlsbad, CA, USA) at 37 °C in a 5% CO_2 atmosphere.

Kinetics of DC transport in HEK293T cells

HEK293T cells were seeded on sterile 96-well black-walled, clear-bottom plates (Corning Inc., Corning, NY, USA) at a density of 1.5×10^4 cells/well. Cells were loaded for 1 h at 37 °C with 5 µM Fura-2 AM or calcein-AM in reaction buffer (RB) composed of 10 mM Hepes (pH 7.4), 120 mM choline chloride, 5 mM KCl, 1 mM $MgCl_2$ and 5 mM D-glucose. This buffer contained choline chloride instead of NaCl to minimize the effect of the Ca^{2+}/Na^+ exchanger. After dye loading, plates were washed twice with RB and 100 µl of RB plus 1 µM thapsigargin (TG) was added to the samples. TG specifically inhibits the sarco(endo)plasmic reticulum Ca^{2+}-ATPase (SERCA) which produces depletion of endoplasmic reticulum (ER) Ca^{2+} stores and the activation of SOCs (Thastrup et al. 1989). Fluorescence was measured at λexcitation 340 ± 11 and 380 ± 20 nm (λemission 500 ± 20 nm) in a fluorometric plate reader (Synergy HT. Biotek, BioTek Instruments Inc., Winooski, VT, USA). Fluorescence signals were analyzed using the software Gen 5.2.01. Stable baseline values were established for at least 2 min, and then, 15 µl of RB containing 1 mM DC (except for Pb^{2+} that was assessed at 100 µM concentration) was added. Traces showing the time course of fluorescence intensity variation were normalized to the baseline values and expressed as relative DC in cytoplasm ($[DC^{2+}]_{Cyt}$).

For Co^{2+} transport measurements, the same procedure was applied, except that cells were loaded with 5 µM calcein-AM instead of Fura-2 AM. Fluorescence was recorded at λemission 485 ± 20 nm (λexcitation 528 ± 20 nm) (Breuer et al. 1995).

Preparation of erythrocyte inside-out vesicles (eIOVs)

Sealed eIOVs were prepared from human erythrocyte plasma membrane as described previously (Steck et al. 1970). After preparation, eIOVs were washed three times with 100 volumes of 1 mM Tris–HCl (pH 8.5) buffer to eliminate the excess of Ca^{2+} and EGTA.

Purification of functional PMCA from human erythrocytes

PMCA was isolated from CaM-depleted human erythrocyte membranes using a CaM-affinity chromatography column (Niggli et al. 1979). After purification, the enzyme was suspended in a solution containing 20% (w/v) glycerol, 120 µM $C_{12}E_{10}$, 120 mM KCl, 1 mM $MgCl_2$, 10 mM HEPES-K (pH 7.4), 2 mM EGTA and 2 mM dithiothreitol, and the preparations were stored in liquid nitrogen until their use.

For the determination of the effects of Pb^{2+}, Co^{2+}, Cd^{2+} and Be^{2+} on PMCA ATPase activity, PMCA-rich preparation was dialyzed prior to its use against 1000 volumes of 10 mM HEPES-K (pH 7.4) buffer containing 120 mM choline, 20% (w/v) glycerol, 120 µM $C_{12}E_{10}$ and 2 mM dithiothreitol at 4 °C to remove EGTA. After the dialysis, PMCA maintained at least 90% of its activity. In addition, the solutions of KCl and MOPS were treated batch-wise with Chelex-100, thus decreasing the concentration of Ca^{2+} in the solutions to 0.10–0.30 µM (Liu et al. 1997). Using this approach, it was possible to adjust the final concentration of free Sr^{2+} and Ba^{2+} to the desired amounts, because the dissociation constants of Sr^{2+}- and Ba^{2+}-EGTA complexes (K_D 0.118 and 0.119 M, respectively) are higher than that of Ca^{2+}-EGTA complex (K_D 0.091 M). Hence, these DCs will not displace Ca^{2+} from its complex with EGTA and the concentration of free DC in the reaction media will remain unmodified. Conversely, the K_D for Pb^{2+}-, Co^{2+}- and Cd^{2+}-EGTA complexes (0.068, 0.081 and 0.060 M, respectively) is smaller than the K_D of Ca^{2+}-EGTA, thus releasing Ca^{2+} from the Ca^{2+}-EGTA complex.

Measurement of DC transport in eIOVs

DC transport was investigated in eIOVs by measuring the intensity of the light scattered (Rossi and Schatzmann 1982), a sensitive method that avoids the use of radioactive isotopes.

Experiments were performed at 37 °C in a media containing eIOVs (70 µg protein/ml) suspended in 30 mM MOPS (pH 7.4) buffer added with 120 mM KCl, 3.5 mM $MgCl_2$ and the appropriate amounts of $CaCl_2$ or the desired DC to obtain the concentration of free cation indicated for the individual experiments. The reaction was initiated by the addition of 2 mM ATP, and light scattering intensity was

measured at 90º scattering angle and recorded in a Jasco FP-6500 spectrofluorometer (λexcitation 490 ± 2.5 nm, λemission 515 ± 5 nm). The relative change in light scattering $\left(\Delta I/I_0\right)$ was calculated using the following equation:

$$\frac{\Delta I}{I_0} = \frac{I - I_0}{I_0} \quad (1)$$

where I_0 and I are the scattered light intensities recorded at time zero and at each experimental time point, respectively. Since variations in light scattering of human erythrocyte eIOVs preparations are related to changes in their volume (Rossi and Schatzmann 1982), it can be verified that:

$$\frac{\Delta I}{I_0} = k\,\frac{\Delta V}{V_0} \quad (2)$$

where $\Delta V/V_0$ is the relative volume change and k is a proportionality factor. Also, as the change in eIOVs volume is proportional to Ca^{2+} transport, the change in light intensity in eIOVs incubated in the presence of the different DCs is a direct measurement of their transport into the vesicles.

Measurement of ATPase activity

PMCA ATPase activity in the samples was calculated from inorganic phosphate release through the hydrolysis of ATP (Fiske and Subbarow 1925). Briefly, PMCA was resuspended in micelles containing 80 μM $C_{12}E_{10}$ and 38 μM PC. The determination of PMCA activity was performed at 37 °C in a 30 mM MOPS (pH 7.4) buffer containing 120 mM KCl, 3.5 mM $MgCl_2$, 2 mM ATP and the amounts of DC necessary to achieve the desired final concentration of the free cation. For the experiments involving the use of PMCA activators, 120 nM CaM was added to the medium to attain the maximal ATPase activity, or PC in the micelles was replaced by PS.

Calculation of free DC concentration in the media

Free cation concentration in the incubation media was estimated using the software Max Chelator (Brooks and Storey 1992).

PMCA labeling with [^{125}I]TID-PC/16

[^{125}I]TID-PC/16 was prepared as described by Mangialavori et al. (2009). A dried film of the photoactivatable reagent was suspended in micelles of PC and $C_{12}E_{10}$ (80 and 120 μM, respectively) containing 10 μg/ml of purified PMCA and suspended in 30 mM MOPS-K (pH 7.2) buffer containing 120 mM KCl, 3.75 mM $MgCl_2$ and the amount of DC to achieve the concentrations indicated for the individual experiments. Samples were incubated for 20 min at 37 °C before being irradiated with UV light (λ 360 nm) for 15 min. Quantification of total and labeled protein was carried out as previously described (Mangialavori et al. 2009).

Proteolysis of PMCA

Controlled proteolysis of PMCA was performed incubating the protein for 5 min at 37 °C in the presence of 25 mM Tris–HCl (pH 7.4) buffer containing 0.1 mM $CaCl_2$ and 0.22 μg/ml of *N*-α-tosyl-L-lysine chloromethyl ketone (TLCK)-treated chymotrypsin (Mangialavori et al. 2010). The reaction was stopped by adding tenfold excess of ovomucoid trypsin inhibitor solution at 4 °C.

Calmodulin (CaM) fluorescence spectroscopy

Samples containing 5 μM CaM in 30 mM MOPS (pH 7.2) buffer and 120 mM KCl were titrated by sequential addition of 0.6–1.5 μl of DC stock solutions (3–15 mM). Changes in CaM tyrosine fluorescence were recorded at 307 ± 5 nm (λexcitation 280 ± 2.5 nm) (Chao et al. 1984).

Data analysis

Theoretical equations were fitted to experimental data by nonlinear regression based on the Gauss–Newton algorithm and using the commercial software Excel and Sigma-Plot for Windows. One-way analysis of variance (ANOVA) followed by Fisher's PLSD (protected least square difference) test was performed using GraphPad Prism version 6.00 for Windows, GraphPad Software (San Diego, CA, USA). A probability (P) value <0.05 was considered statistically significant. The number of independent experiments (n) is indicated in each figure legend.

Results

Transport of Ca^{2+} and toxic DCs in HEK293T cells

The uptake of Ca^{2+} and DCs in intact HEK293T cells was evaluated by measuring the kinetics of Fura-2 fluorescence. Cells were loaded with the probe and further incubated in the presence of 1 μM TG to empty Ca^{2+} stores at the endoplasmic reticulum and cause SOCs activation. The activity of Ca^{2+}/Na^+ exchanger was minimized throughout the experiments due to the absence of Na^+ in the extracellular milieu. Samples were next added with the DCs, and the kinetics of Fura-2 fluorescence variation was evaluated. As expected, the addition of Ca^{2+} to the incubation media caused rapid increase in Fura-2 fluorescence (Fig. 1a) that reached a maximum within the first minute of incubation. At prolonged incubation times, Fura-2 fluorescence decreased

progressively, indicating the efflux of Ca^{2+} from cytoplasm. In parallel, experiments were performed in the presence of La^{3+} to inhibit the activity of SOCs (Bouron et al. 2005). As shown in Fig. 1a, La^{3+} completely abolished Ca^{2+} entry, thus indicating that these channels were involved in Ca^{2+} uptake in HEK293T cells upon TG-mediated Ca^{2+} depletion. As observed for Ca^{2+}, Sr^{2+}, Ba^{2+}, Pb^{2+} and Cd^{2+} also caused rapid increase in Fura-2 fluorescence, an effect that was totally (Sr^{2+}, Ba^{2+}, Pb^{2+}) or partially (Cd^{2+}) prevented by SOCs inhibition with La^{3+} (Fig. 1b–e). The latter observation suggests that, in addition to SOCs, Cd^{2+} may use a different transporter/channel to reach cell cytoplasm. Like Ca^{2+}, Sr^{2+} also exited cells although with lower rate (Fig. 1b). In contrast, the uptake of Ba^{2+}, Pb^{2+} and Cd^{2+} occurred throughout the experiment, as evidenced from the continuous increase in the fluorescence of Fura 2-DC complex (Fig. 1c–e). In the case of Be^{2+}, its entry was almost negligible (~20% of maximal Ca^{2+} uptake) and not preventable by La^{3+} (Fig. 1f). It reached a plateau after 2 min of incubation, with no evidences of spontaneous exit from cells (Fig. 1f).

Co^{2+} uptake could not be measured because Co^{2+} forms a high-affinity (K_D 8.6 nM) non-fluorescent complex with Fura-2 that prevented these measurements (Kwan and Putney

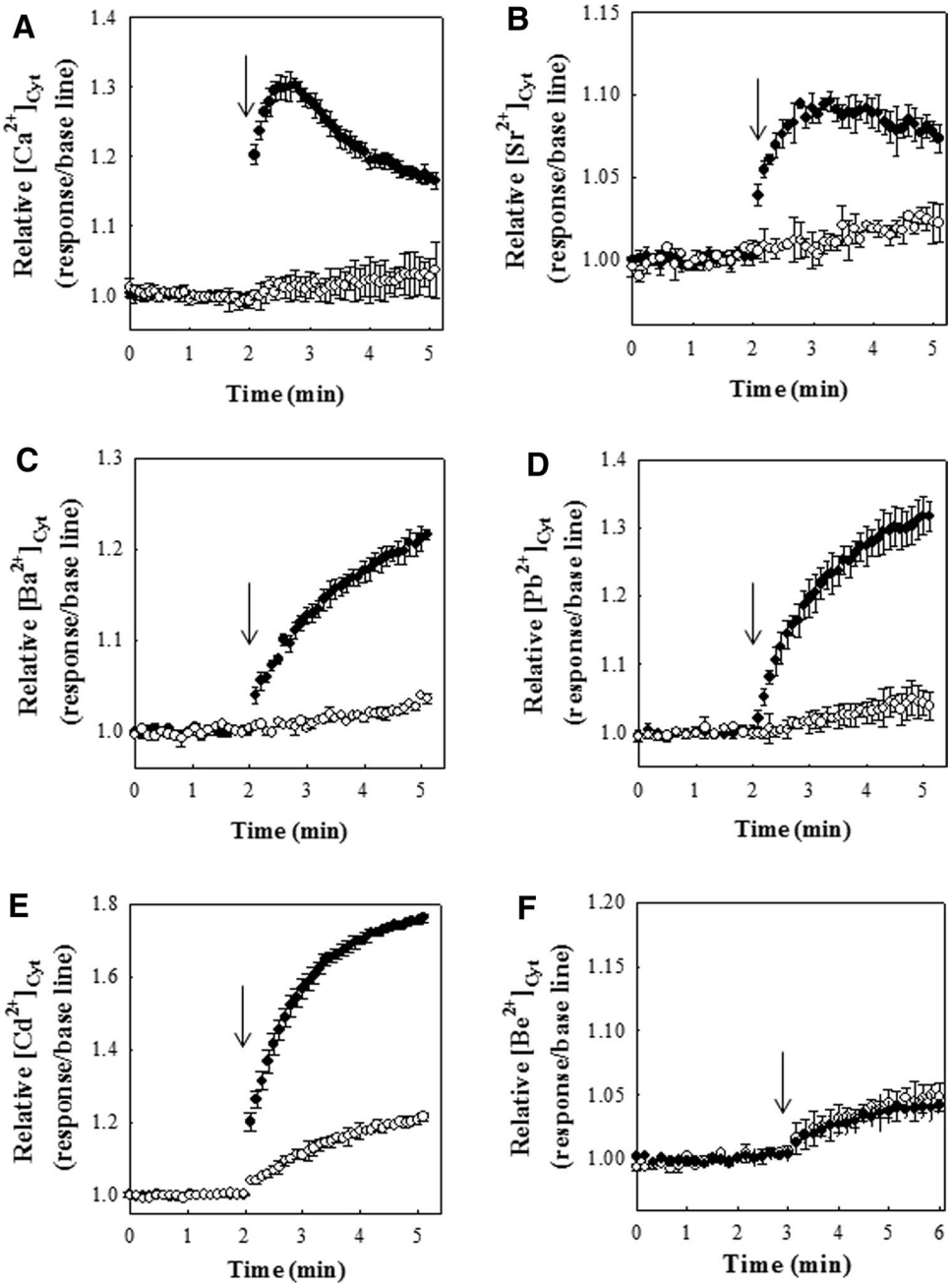

Fig. 1 SOCs participate in Ca^{2+} and DCs entry in Ca^{2+} stores-depleted HEK293T cells. HEK293T cells were loaded with the fluorescent probe Fura-2 and pre-incubated for 30 min with 1 μM TG either in the absence (*closed circles*) or in the presence (*open circles*) of 100 μM La^{3+}, and baseline fluorescence was recorded for at least 2 min. *Arrows* indicate the moment when **a** Ca^{2+}, **b** Sr^{2+}, **c** Ba^{2+}, **d** Pb^{2+}, **e** Cd^{2+} or **f** Be^{2+} were added to the samples. All the DCs were assessed at 1 mM concentration, except Pb^{2+} (100 μM). The kinetics of DC entry was evaluated from the increase in Fura-2 fluorescence intensity. Results are shown as the mean ± SD ($n = 3$)

1990). Accordingly, the addition of this DC to the samples caused very small but rapid decrease in Fura-2 fluorescence which returned to baseline values at prolonged incubations and that was not prevented by La^{3+} (Suppl. Fig. 1). Thus, a different fluorescent probe was used to assess Co^{2+} entry, calcein which binds Co^{2+} reversibly, rendering a non-fluorescent complex (Breuer et al. 1995). The addition of Co^{2+} to calcein-loaded cells caused large and rapid decrease in its fluorescence that reached a plateau after 6 min of incubation (Fig. 2). In contrast to the other DCs investigated, the addition of La^{3+} to the incubation media partially prevented Co^{2+} entry (Fig. 2). The kinetics of Co^{2+} entry ($[Co^{2+}]_t$) in the absence and in the presence of La^{3+} were described by the following equation:

$$\left[Co^{2+}\right]_t = \left(\left[Co^{2+}\right]_{t0} - \left[Co^{2+}\right]_{t\infty}\right) \times e^{(-kt)} + \left[Co^{2+}\right]_{t\infty} \quad (3)$$

where $[Co^{2+}]_{t0}$ and $[Co^{2+}]_{t\infty}$ are the minimal and maximal relative amount of intracellular Co^{2+}, respectively, and k is the first-order rate constant. The comparison of fitting parameters by Akaike's information criteria indicated that maximal Co^{2+} concentration achieved within cells and the influx rate constant were different in both experimental situations, thus suggesting that this DC uses different transporters to reach cells.

To evidence more clearly the exit of DCs from cells, once DC-Fura-2 complex formation reached its maximum, 2.5 mM EGTA was added to the samples to prevent the re-internalization of the DCs. Accordingly, the decrease in Fura-2-Ca^{2+} complex fluorescence was markedly higher in the presence of EGTA (Fig. 3a) than in its absence (Fig. 1a).

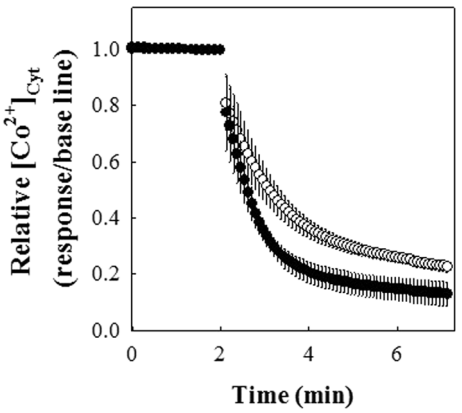

Fig. 2 Co^{2+} entry in HEK293T is not mediated exclusively by SOCs. HEK293T cells were loaded with the fluorescent probe calcein and pre-incubated for 30 min with 1 µM TG, either in the absence (*closed circles*) or in the presence (*open circles*) of 100 µM La^{3+}, and baseline fluorescence was recorded for 2 min. The *arrow* indicates the moment when 1 mM Co^{2+} was added to the samples. The kinetics of DC entry was evaluated from the decrease in calcein fluorescence intensity. Results are shown as the mean ± SD ($n = 3$)

Similar results were obtained for cells exposed to Sr^{2+} (Fig. 3b). In Ba^{2+}-, Pb^{2+}-, Cd^{2+}- or Be^{2+}-treated cells, the decrease in Fura-2-DC complex fluorescence in the presence of EGTA was minimal (Fig. 3c–f), indicating that the velocities of exit of these DCs were minor respect to that of Ca^{2+}. Similarly, the fluorescence of calcein-loaded cells exposed to Co^{2+} was only slightly increased upon EGTA addition, evidencing the tendency of this metal to accumulate within cells (Fig. 4).

Transport of Ca^{2+} and toxic DCs in eIOVs

The obtained results in HEK293T cells indicate that the assessed DCs can reach cell cytoplasm, although their exit from cells was much lower than that of Ca^{2+}. Considering that PMCA is the main Ca^{2+} transporter at the plasma membrane and that Ca^{2+}/Na^{+} exchanger activity was minimized, we next performed a series of experiments to determine the capacity of PMCA to transport the DCs using two in vitro models: eIOVs and purified PMCA.

The transport of Ca^{2+} in eIOVs was evaluated by measuring the kinetics of light scattering variations (Rossi and Schatzmann 1982). According to this method, the uptake of Ca^{2+} produces an enlargement of the vesicles with the consequent decrease in the amount of light scattered, which is proportional to the concentration of Ca^{2+} within the vesicles (Rossi and Schatzmann 1982). This experimental approach was then used to quantify the amount of DC transported by PMCA into the eIOVs.

To verify that Ca^{2+} uptake occurred in the current experimental conditions, the kinetics of light scattering change ($\Delta I/I_0$) were recorded for eIOVs preparations incubated in either the absence or presence of 80 µM Ca^{2+} (Fig. 5a). Samples were first incubated for 1800 s to identify the kinetics of the passive entry of Ca^{2+} in an ATP-independent process. This value was used as reaction blank that was subtracted from the ATP-dependent process, initiated by the addition of 2 mM ATP. The subsequent addition of the ionophore A23187 returned the scattered light intensity toward a value close to that measured in samples incubated in the absence of Ca^{2+}. This result confirmed that the change in light scattering was caused by the specific uptake of Ca^{2+} into the eIOVs.

Linear functions were adjusted to data obtained in the presence of Ca^{2+} and in the absence of ATP (initial part of black curve, Fig. 5a), or in the absence of Ca^{2+} and in the presence of ATP (gray curve, Fig. 5a). The finding that both slopes were similar [$(2.01 \pm 0.05)\ 10^{-5}$ and $(3.1 \pm 0.05)\ 10^{-5}\ \Delta I/I_0\ s^{-1}$, respectively] indicates that the spontaneous decay in light scattering observed was not caused by the uptake of Ca^{2+} via PMCA, since this process strictly depends on ATP hydrolysis.

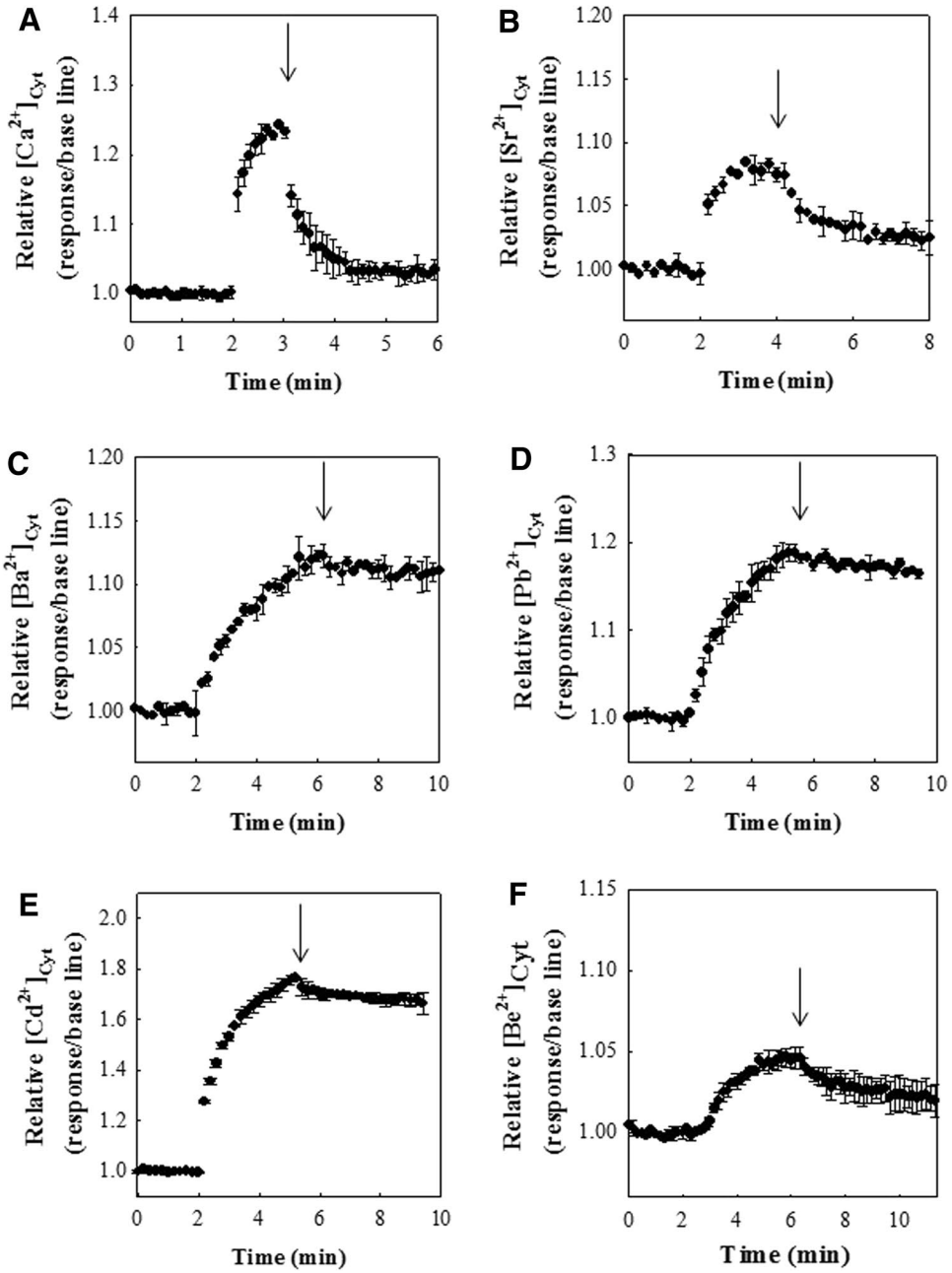

Fig. 3 Ca^{2+} and DCs efflux from HEK293T cells occurs at different rates. HEK293T cells were loaded with the fluorescent probe Fura-2, pre-incubated in the conditions indicated in Fig. 1 and incubated in the presence of **a** Ca^{2+}, **b** Sr^{2+}, **c** Ba^{2+}, **d** Pb^{2+}, **e** Cd^{2+} or **f** Be^{2+}. All the DCs were assessed at 1 mM concentration, except Pb^{2+} (100 µM). At the time indicated by the *arrow*, 2.5 mM EGTA was added to the samples and fluorescence intensity was recorded until attaining stable values. Results are shown as the mean ± SD ($n = 3$)

When eIOVs were incubated in the presence of 80 µM Ca^2, the addition of ATP produced an exponential decrease in the amount scattered light that can be described by Eq. 4:

$$\frac{\Delta I}{I_0} = \left(\frac{\Delta I}{I_0}\right)_{\infty} + Ae^{-kt} \quad (4)$$

where $(\Delta I/I_0)_\infty$ is the change in light scattering intensity when time tends to infinity, A is the maximal change of light scattering intensity and k is the rate coefficient. The best-fitting values of the parameters were $(\Delta I/I_0)_\infty$ −0.430 ± 0.002, A 0.631 ± 0.001 and k (3.082 ± 0.026) 10^{-4} s^{-1}. The initial rate of Ca^{2+} transport—calculated as the product between A and k—was 1.2 ± 0.02 10^{-4} s^{-1} (Rossi and Schatzmann 1982). The rates of light scattering change and the Ca^{2+}-ATPase activity were measured at different Ca^{2+} concentrations (Fig. 5b), and experimental data were described by a rectangular hyperbola (Eq. 5):

$$V = \frac{V_{max}\,[DC]}{K_{0.5} + [DC]} \quad (5)$$

where [DC] denotes the concentration of Ca^{2+} or any other DC assessed in this study, V_{max} is the activity of ATPase when the concentration of the DC tends to infinity, and $K_{0.5}$ represents the apparent affinity of PMCA for the DC.

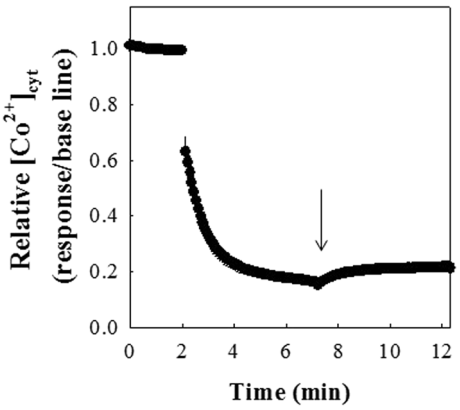

Fig. 4 Co^{2+} efflux from HEK293T cells is minimal. HEK293T cells were loaded with the fluorescent probe calcein, pre-incubated in the conditions indicated in Fig. 2 and incubated in the presence of 1 mM Co^{2+}. At the time indicated by the *arrow*, 2.5 mM EGTA was added to the samples and fluorescence intensity was recorded until attaining stable values. Results are shown as the mean ± SD ($n = 3$)

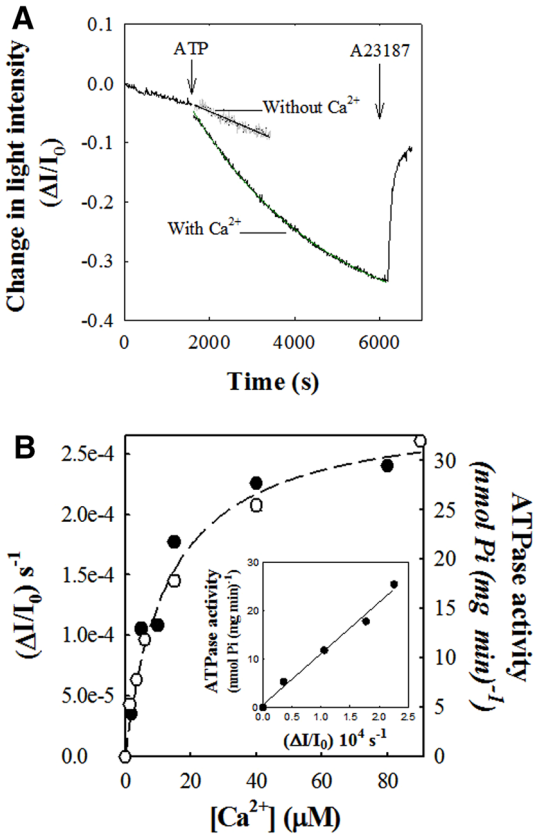

Fig. 5 Ca^{2+}-mediated light scattering variations in eIOVs is a valuable tool for the evaluation of DCs transport. **a** The kinetics of Ca^{2+} (80 μM)-mediated changes in the light scattering of eIOVs preparations was measured. Traces correspond to representative experiments, and the continuous line represents a linear function adjusted to experimental data. **b** Effect of Ca^{2+} concentration on the light scattering variation of eIOVs preparations and on ATPase activity. eIOVs light scattering (*closed circles*) and Ca^{2+}-ATPase activity (*open circles*) were determined in a medium containing 2 mM ATP and the adequate amount of Ca^{2+} to obtain the desired final concentrations of free Ca^{2+} (0-90 μM) in the media. *Dashed line* represents Eq. 5 fitting to experimental data. Results are shown as the mean ± SEM ($n = 3$). The absence of *error bars* indicates error was within size of *symbol*. *Inset* correlation between the ATPase activity of PMCA and Ca^{2+} transport

The similarity between the $K_{0.5}$ values calculated for the measurements of Ca^{2+} transport (10.7 ± 2.4 μM) and Ca^{2+}-ATPase activity (13.0 ± 1.8 μM) indicates that the observed changes in the light scattered by samples in the presence of Ca^{2+} and ATP is a direct measurement of PMCA activity. In fact, a linear relationship (r^2 0.99, $P < 0.001$) was observed between both parameters (inset to Fig. 5b).

Next, we investigated whether the pump was also able to transport others DCs, e.g., Sr^{2+}, Ba^{2+}, Co^{2+}, Cd^{2+}, Pb^{2+} and Be^{2+}. For each condition, eIOVs were pre-incubated in the reaction media without (control) or with the desired DC and the reaction was initiated by the addition of ATP as indicated previously. As observed for Ca^{2+}, light scattering variations for eIOVs incubated in the presence of the DCs were described by rectangular hyperbolas, indicating saturable, ATP-dependent process (data not shown). The rate of DC transport was expressed as the percentage of the value measured for Ca^{2+} (Table 1). Results indicate that in the current conditions, PMCA transported equally Ca^{2+} and Sr^{2+}. In contrast, the transport of Co^{2+} and Pb^{2+} was markedly lower respect the value obtained for Ca^{2+} ($P < 0.001$, ANOVA). The values obtained for Cd^{2+} and Ba^{2+} transport can be considered marginal and within the experimental error of the determination. No detectable transport of Be^{2+} was observed in the current experimental conditions (Table 1).

Effects of DC on PMCA ATPase activity in the absence of activators

The ATPase activity in the purified PMCA preparation was measured at different concentrations of Ca^{2+}, Sr^{2+}, Ba^{2+} or Be^{2+} (Fig. 6a), or Co^{2+}, Pb^{2+} or Cd^{2+} (Fig. 6b). Like Ca^{2+}, experimental data obtained for the Sr^{2+} and Ba^{2+} were described by Eq. 5. Whereas samples containing Ca^{2+} or Sr^{2+} had similar $K_{0.5}$ and V_{max} values, those containing Ba^{2+} had higher $K_{0.5}$ and lower V_{max} values (Table 2). No ATPase activity was detected in the presence of Be^{2+} (Fig. 6a). PMCA ATPase activity measured in the presence of Co^{2+} or Pb^{2+} (Fig. 6b) was best described by Eq. 6:

$$V = \frac{V_{max}\,[DC]^n}{[K_{0.5}]^n + [DC]^n} \quad (6)$$

where "n" is the Hill coefficient. Interestingly, the values of $K_{0.5}$ and V_{max} calculated for Co^{2+}- and Pb^{2+}-containing

Table 1 ATP-dependent uptake of DCs by eIOVS

DC	$(\Delta I/\Delta I_0\ s^{-1})$ (%)
Ca^{2+}	100.0 ± 1.7[a]
Sr^{2+}	113.5 ± 2.5[a]
Pb^{2+}	54.6 ± 4.9[b]
Co^{2+}	24.5 ± 6.1[b]
Cd^{2+}	10.6 ± 4.5[b]
Ba^{2+}	10.1 ± 6.3[b]
Be^{2+}	ND

DC transport was calculated from the kinetics of light scattering variation ($\Delta I/I_0\ s^{-1}$). Results are relativized to the value measured for Ca^{2+} and are expressed as the mean ± SEM ($n \geq 3$). *ND* non-detectable. Results having different superscripts are significantly different ($P < 0.001$, ANOVA)

samples were lower than those calculated for Ca^{2+} (Table 2). For these DC, Hill coefficients were higher than the unity, suggesting that two or more cations must bind to the PMCA to activate it.

In contrast to the observed for the other DC assessed, the ATPase activity of PMCA incubated in the presence of Co^{2+} or Pb^{2+} showed biphasic behavior, with an activation phase attained at low DC concentrations, followed by an inhibition phase (Fig. 6b). Worth of noticing, no ATPase activity was detected in the presence of Cd^{2+} (Fig. 6b). Since Cd^{2+} competes with Ca^{2+} for its binding to the ATPases (Yuan et al. 2013), we evaluated the effects of Cd^{2+} on Ca^{2+}-ATPase activity, in both the absence and presence of dithiothreitol (DTT). In the absence of DTT, Cd^{2+} abolished Ca^{2+}-ATPase activity, an effect that was observed at 5 μM Cd^{2+} and higher concentrations (Fig. 7). This inhibitory effect of Cd^{2+} was partially prevented by DTT. In these conditions, the inhibition constants (Ki_{Cd}) for samples incubated in the absence or presence of DTT were 2.7 ± 0.2 and 18.0 ± 1.4 μM, respectively (Fig. 7). When Ca^{2+} concentration was fixed at 10 μM and DTT was present in the media, the Ki_{Cd} was 8 ± 2 μM (inset to Fig. 7). Since DTT can only protect the most superficial –SH groups in PMCA (Vats et al. 2002), these results suggest that in addition to those, Cd^{2+} could also bind to sterically less accessible –SH groups and/or to Ca^{2+} binding site in PMCA, thus inhibiting its ATPase activity through mixed mechanisms.

Effects of the DC on the conformation of PMCA transmembrane domains

[^{125}I]TID-PC/16 is a lipophilic probe that evaluates the exposure of protein transmembrane domains to lipids and allows

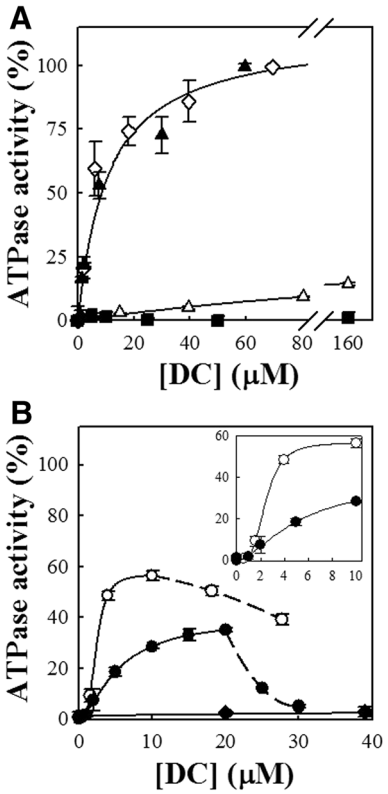

Fig. 6 DCs affect differently PMCA ATPase activity. ATPase activity was measured using purified PMCA preparations incubated in the presence of increasing concentrations of **a** Ca^{2+} (*closed triangles*), Sr^{2+} (*open diamonds*), Ba^{2+} (*open triangles*) or Be^{2+} (*closed squares*), or **b** Co^{2+} (*open circles*), Pb^{2+} (*closed circles*) or Cd^{2+} (*closed diamonds*). Experimental data were relativized to PMCA activity measured at 80 μM Ca^{2+}. Continuous lines represent the fitting of **a** Eq. 5 and **b** Eq. 6 to experimental data using the fitting parameters shown in Table 2. Discontinuous lines represent the fitting of an empirical equation to experimental data. Results are shown as the mean ± SEM ($n \geq 3$). *Inset* detail of PMCA activity measured at low concentrations of Co^{2+} (*open circles*) and Pb^{2+} (*closed circles*) (0–10 μM)

evidencing two different conformations of PMCA (Mangialavori et al. 2009). The first one, with maximal exposure to lipids, corresponds to the auto-inhibited state of the enzyme (E_1-Ca). The second conformation, with minimal exposure to lipids, corresponds to the conformation E_2 (Mangialavori et al. 2009). On this basis, we investigated whether, similarly to Ca^{2+}, the DC assessed may cause conformational changes in PMCA transmembrane domains.

The specific incorporation of [^{125}I]TID-PC/16 to purified PMCA was 55% higher when measured in the presence of Ca^{2+} than in its absence (EGTA, Fig. 8). Sr^{2+}, Pb^{2+} and Co^{2+} caused PMCA labeling similar to that observed for Ca^{2+} (150.8 ± 12.4, 140.6 ± 3.7 and 132.1 ± 3.1%, respectively), whereas Ba^{2+} and Cd^{2+} caused a labeling similar to that obtained for samples treated with EGTA (98.1 ± 4.8 and 98.5 ± 15.9%, respectively) (Fig. 8). The effect of Be^{2+}

Table 2 Effect of DCs on the kinetic parameters of ATPase activity of purified PMCA and measured in the absence or presence of known PMCA activators

DC	Activator	V_{max} (%)	$K_{0.5}$ (μM)	Catalytic efficiency (% μM^{-1})
Ca^{2+}	None	113.3 ± 6.7^a	10.8 ± 2.3^a	10.5 ± 2.9^a
	CaM	133.7 ± 5.6^a	1.2 ± 0.2^d	111.4 ± 23.2^b
	Proteolysis	140.2 ± 7.2^c	1.5 ± 0.4^c	93.5 ± 29.8^b
	PS	130.0 ± 2.2^a	1.7 ± 0.1^c	76.5 ± 5.8^c
Sr^{2+}	None	108.9 ± 3.7^a	8.7 ± 1.3^a	12.5 ± 2.3^a
	CaM	149.4 ± 3.2^c	2.9 ± 0.3^d	51.5 ± 6.4^b
	Proteolysis	147.0 ± 2.2^c	1.3 ± 0.1^d	113.1 ± 10.4^b
Ba^{2+}	None	24.5 ± 2.1^b	95.1 ± 15.6^b	0.3 ± 0.1^c
	CaM	NC	NC	NC
	Proteolysis	48.2 ± 2.9^a	50.2 ± 7.4^b	0.96 ± 0.20^e
Co^{2+}	None	56.7 ± 0.7^b	2.4 ± 0.1^a	23.6 ± 1.3^d
	CaM	117.8 ± 1.8^a	1.87 ± 0.03^a	63.0 ± 2.0^f
Pb^{2+}	None	39.4 ± 1.8^b	5.3 ± 0.5^a	7.4 ± 1.0^a
	PS	35.4 ± 3.3^b	3.3 ± 0.7^a	10.7 ± 3.3^a
Cd^{2+}	None	ND	ND	ND
Be^{2+}	None	ND	ND	ND

Results are expressed as the mean ± SEM ($n \geq 3$). *NC* not calculated, *ND* non-detectable, *CaM* calmodulin, *PS* phosphatidylserine. Results in the same column having different superscripts are significantly different (a vs. b: $P < 0.001$; a vs. c: $P < 0.05$; a vs. d: $P < 0.01$; c vs. e: $P < 0.05$; d vs. f: $P < 0.001$; ANOVA)

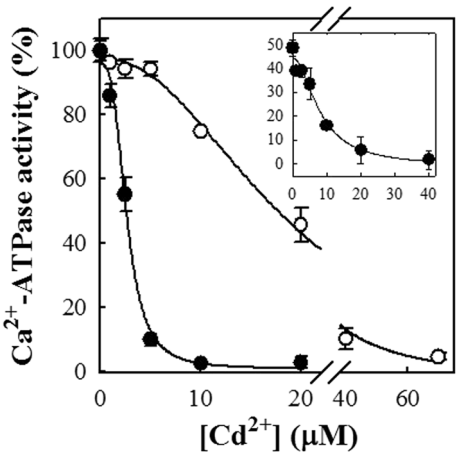

Fig. 7 Cd^{2+} binding to PMCA occurs at different sites with dissimilar inhibitory capacity. Purified PMCA was incubated in the presence of 80 μM Ca^{2+} and increasing amounts of Cd^{2+}, either in the absence (*closed circles*) or in the presence (*open circles*) of 5 mM DTT. Ca^{2+}-ATPase activity was measured. Results are shown as the mean ± SEM ($n \geq 3$). *Inset* effect of Cd^{2+} concentration on Ca^{2+}-ATPase activity measured at 10 μM Ca^{2+} and 5 mM DTT. *Continuous lines* represent the fitting of an empirical equation to experimental data

on PMCA conformation was not evaluated as no PMCA-mediated transport of Be^{2+} (Table 1) and no Be^{2+}-dependent PMCA ATPase activity (Fig. 6) were detected. The finding that Sr^{2+}, Pb^{2+} and Co^{2+} produced a conformational change on PMCA transmembrane domain compatible to the one caused by Ca^{2+} suggests that these cations could bind and drive PMCA to a conformation similar to E_1-Ca. Despite of causing the adequate change in PMCA conformation, Co^{2+} and Pb^{2+} were not transported with the same velocity than Ca^{2+}, and thus, these cations could be considered as partial uncouplers of PMCA activity. In contrast, Ba^{2+} and Cd^{2+} (even in the presence of DTT; data not shown) were unable to drive E_2–E_1, at least in the experimental conditions assessed.

Effects of DC on the conformation of CaM, the main PMCA activator

CaM has two tyrosine residues (Tyr_{99} and Tyr_{138}) that account for its fluorescence. The binding of Ca^{2+} to CaM produces a conformational change in the protein that increases the quantum yield of Tyr fluorescence (Supp. Fig. 2). The subsequent addition of EGTA decreases CaM fluorescence to the initial values, thus demonstrating the specificity of the fluorescence change.

To assess the effects of DCs on purified CaM conformation, the fluorescence intensity of the protein was recorded at different DC concentrations. Results obtained for each condition assessed were relativized to the value obtained

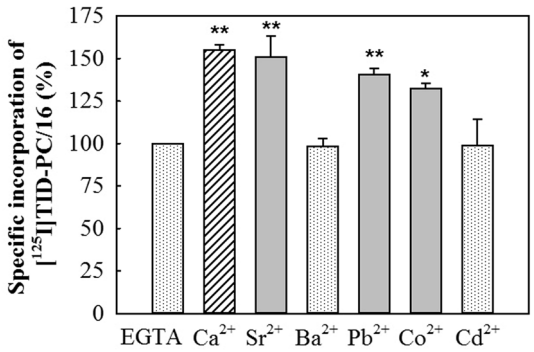

Fig. 8 Ca^{2+}, Sr^{2+}, Ba^{2+} and Co^{2+} induce the change of PMCA transmembrane domains conformation necessary for its functioning. Purified PMCA was incubated in the presence of Ca^{2+} (80 μM), Sr^{2+} (80 μM), Ba^{2+} (160 μM), Pb^{2+} (20 μM), Co^{2+} (10 μM) or Cd^{2+} (20 μM), and the conformation of PMCA transmembrane domains was evaluated from the incorporation of the probe [^{125}I]TID-PC/16. The specific incorporation of the probe in DC-treated PMCA was relativized to the value measured in samples containing 2 mM EGTA. Results are shown as the mean ± SEM ($n \geq 4$). * and ** are significantly different from the value measured in samples containing EGTA ($P < 0.01$ and $P < 0.001$, respectively)

for the optimal concentration of Ca^{2+}/CaM. In the presence of Ca^{2+}, Sr^{2+} or Cd^{2+}, CaM fluorescence increased in a sigmoidal manner (Fig. 9a). Although the concentration of Ca^{2+} and Sr^{2+} necessary to cause half of the maximal fluorescence change ($K_{0.5f}$) was similar (Ca^{2+} 2.07 ± 0.06 mol DC/mol CaM; Sr^{2+} 2.65 ± 0.07 mol DC/mol CaM), the maximal fluorescence attained was slightly lower for Sr^{2+} (84.1%). In contrast, the $K_{0.5f}$ calculated for Cd^{2+} was two times higher (4.9 ± 0.06 mol DC/mol CaM) than that for Ca^{2+}, although their maximal fluorescence values were similar. The sigmoidal behavior observed for these DCs is consistent with the fact that CaM has four sites capable of DC binding. However, and as stated by Chao et al. (1984) "these measurements do not represent the stoichiometry of metal binding nor they relative binding affinity, but their abilities to substitute for Ca^{2+}." Ba^{2+} (Fig. 9a) and Be^{2+} (Fig. 9b) did not induce significant changes in CaM fluorescence along the range of concentrations investigated.

A different behavior was observed for Co^{2+} and Pb^{2+}. Co^{2+} induced a sigmoidal increase in CaM fluorescence (Fig. 9b), with a $K_{0.5f}$ of 17.8 ± 0.2 mol Co^{2+}/mol CaM, 8.5 times higher than the obtained for Ca^{2+}. In contrast, Pb^{2+} showed a biphasic behavior on CaM fluorescence (Fig. 9b). At low Pb^{2+}/CaM molar ratios, the fluorescence of CaM increased in a sigmoidal fashion ($K_{0.5f}$ 15.8 ± 0.2 mol Pb^{2+}/mol CaM), whereas at high Pb^{2+}/CaM molar ratios the fluorescence of CaM decreased abruptly (Fig. 9b).

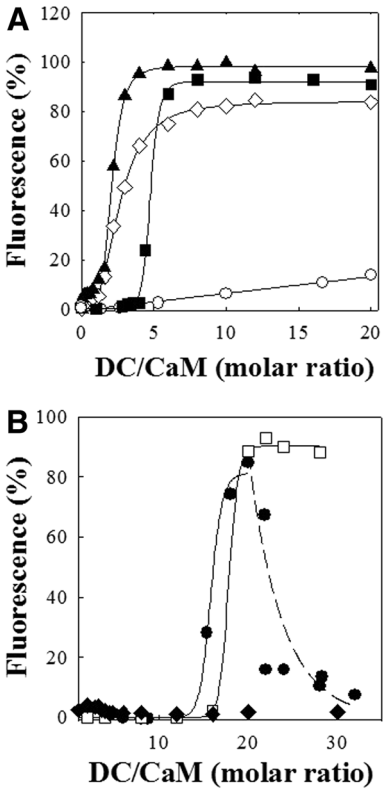

Fig. 9 DCs have different capacity to interact with calmodulin. CaM (5 μM) was incubated in the presence of increasing concentrations of **a** Ca^{2+} (*closed triangles*), Sr^{2+} (*open diamonds*), Cd^{2+} (*closed squares*) or Ba^{2+} (*open circles*), or **b** Co^{2+} (*open squares*), Pb^{2+} (*closed circles*) or Be^{2+} (*closed diamonds*), and CaM fluorescence was recorded. The fluorescence obtained with a saturating Ca^{2+} concentration was taken as 100%. Results are shown as the mean ± SEM ($n \geq 3$). The absence of *error bars* indicates that error was within size of *symbol*

Effects of DCs on PMCA ATPase activity in the presence of PMCA activators

Current results indicate that in vitro, PMCA in its auto-inhibited state transports Sr^{2+}, as well as Co^{2+} and Pb^{2+} although with lower velocities. In addition, PMCA displayed DC-ATPase activity when in the presence of Sr^{2+}, Ba^{2+}, Co^{2+} and Pb^{2+} but not when in the presence of Cd^{2+} or Be^{2+}. To characterize further the effects of DCs on PMCA ATPase activity, experiments were repeated in the presence of physiological PMCA activators. As mentioned in "Introduction," CaM and acidic phospholipids increase the apparent affinity for Ca^{2+} binding, causing maximal ATPase activity, while the removal of the auto-inhibitory domain of PMCA leads the pump to an irreversible activated state. The selection of the activators assessed for each DC was based on their effect on CaM fluorescence (see above).

First, PMCA was added with 120 nM CaM, and the effects of Ca^{2+}, Sr^{2+}, Ba^{2+} or Co^{2+} (0–90 μM) on ATPase activity were evaluated (Fig. 10a). As expected, CaM slightly increased V_{max} value of PMCA measured in the presence of Ca^{2+}, but caused major changes in the $K_{0.5}$ for this cation and the catalytic efficiency of the enzyme (Table 2). For samples incubated in the presence of Co^{2+}, CaM caused 2- and 2.7-fold increase in V_{max} and catalytic efficiency values, respectively, but without affecting $K_{0.5}$ (Table 2). CaM also increased V_{max} and $K_{0.5}$ for Sr^{2+}, although its effect on the catalytic efficiency of the enzyme was lower than the observed for Ca^{2+} (Table 2). Since ATPase activity of PMCA increased linearly with Ba^{2+} concentration (Fig. 10a), the kinetic parameters could not be calculated for this cation (Table 2).

Next, the ATPase activity of chymotrypsin-proteolyzed PMCA was measured in the presence of Ca^{2+}, Sr^{2+} and Ba^{2+} (Fig. 10b). The kinetic parameters calculated for Ca^{2+} and Sr^{2+} (using Eq. 5) were close to those obtained in the presence of CaM (Table 2). In contrast to the observed for CaM-activated PMCA, it was possible to calculate V_{max} for Ba^{2+} under these experimental conditions. The analysis of the kinetic parameters indicates that the proteolysis of PMCA increased twofold both the V_{max} and the apparent affinity for Ba^{2+} respect to the values calculated for the non-activated PMCA and suggests that PMCA could transport Ba^{2+} but with very low apparent affinity and velocity.

Since Pb^{2+} interfered with CaM conformation (Fig. 9b), and being impossible to use EGTA-containing buffers for these measurements because Pb^{2+} displaces Ca^{2+} from its EGTA complex, the effect of a different activator of PMCA was assessed for this cation, the acidic phospholipid PS (Fig. 10c). As expected, PS increased seven times the catalytic efficiency of PMCA, as well as its apparent affinity for Ca^{2+} (Table 2). Whereas the experimental data obtained for Ca^{2+} were described by Eq. 5, data obtained for Pb^{2+} were best described by Eq. 6. In contrast to the observed for Ca^{2+}, PS did not affect the kinetic parameters obtained for Pb^{2+} (Table 2). As observed in the absence of activators (Fig. 6a), no ATPase activity was recorded in the presence of Be^{2+} (Fig. 10c).

Discussion

During its reaction cycle, PMCA undergoes a series of conformational changes that allow the transport of Ca^{2+} from the cytoplasm to the extracellular milieu. This process requires that the intermediaries of the reaction cycle adopt proper conformations. In this work, we demonstrated that similarly to Ca^{2+}, Sr^{2+}, Pb^{2+} and Co^{2+} increase the area of PMCA accessible to the surrounding lipids, which suggests that they induce PMCA to adopt the correct conformation for its phosphorylation, creating a conformational environment adequate for DC transport. As expected, Sr^{2+} was transported in vitro by purified PMCA with kinetic parameters close to those for Ca^{2+} transport, but the transport of Pb^{2+} and Co^{2+} had maximal velocities that were less than half of that measured for Ca^{2+}. Conversely, Ba^{2+} and Cd^{2+}, that did not induce PMCA conformational change, were not transported by the pump. These results do not indicate necessarily that Ba^{2+} and Cd^{2+} do not bind to PMCA. Instead, their binding to PMCA may occur in sites different from Ca^{2+}-binding site, and/or the resulting E_1-Cd^{2+} and E_1-Ba^{2+} conformations may be different from that of E_1-Ca^{2+}. Because of any of these hypothetical situations, PMCA will remain in a non-functional state.

The capacity of certain DC to replace Ca^{2+} from its binding proteins has been related to the similarity between their ionic radii and that of Ca^{2+}. Supporting that, and similar to the observed for the sarco/endoplasmic reticulum Ca^{2+}-ATPase (SERCA) (Sumida et al. 1986), the ATPase activity of PMCA was stimulated by several DCs. The effects of the DCs on ATPase activity of auto-inhibited and activated PMCA followed bell-shaped dependences on DC ionic radii (Fig. 11). The Gaussian curves were centered at 1.110 Å (r^2 0.85) and 1.097 Å (r^2 0.73) for the auto-inhibited and activated states, respectively, which are close to the ionic radius of hexavalent Ca^{2+} (1.09 Å). Additionally, activated PMCA transports other DCs, provided their ionic radii lie in the 0.84–1.35 Å range. However, we detected an exception to this rule, Cd^{2+} that, despite having an adequate ionic radius, cannot be transported by PMCA.

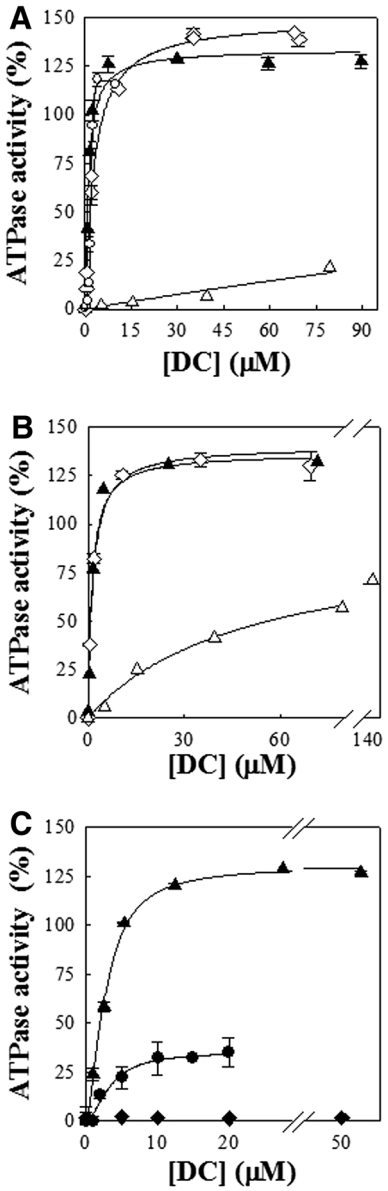

Fig. 10 Classical PMCA activators have dissimilar influences on DCs-dependent ATPase activity. Samples containing **a** CaM (120 nM)-activated PMCA, **b** chymotrypsin-proteolized PMCA, or **c** PMCA reconstituted in PS-containing micelles were obtained. Samples were incubated in the presence of: **a** Ca^{2+} (*closed triangles*), Sr^{2+} (*open diamonds*), Ba^{2+} (*open triangles*) or Co^{2+} (*open circles*); **b** Ca^{2+} (*closed triangles*), Sr^{2+} (*open diamonds*) or Ba^{2+} (*open triangles*); **c** Ca^{2+} (*closed triangles*), Pb^{2+} (*closed circles*) or Be^{2+} (*closed diamonds*). At the end of incubation, PMCA ATPase activity was evaluated. Results are shown as the mean ± SEM ($n \geq 3$). Continuous lines represent the fitting of **a**, **b** Eq. 5, or **c** Eq. 6 to the experimental data, using the fitting parameters shown in Table 2

Cd^{2+} is an extremely toxic metal, capable of causing severe damage to the organs (Jarup and Akesson 2009).

Particularly, its accumulation in the nervous system has been proposed as an etiological factor of Alzheimer's and Parkinson's diseases, and other neurodegenerative disorders. However, the evidences supporting Cd^{2+} involvement in these diseases are still inconclusive (Akatsu et al. 2012; Panayi et al. 2002). The uptake of Cd^{2+} does not compete with Ca^{2+} entry (Verbost et al. 1989) and is mediated by the DC transporters SLC39, SLCA11A2 and certain members of the ABC family (Thevenod 2010). Our experiments in HEK293T cells indicate that Cd^{2+} uptake proceeds mainly—but not exclusively—via SOCs, since its entry was only partially inhibited by La^{3+}. The subsequent accumulation of Cd^{2+} within cells could occur for multiple reasons. Among others, being the affinity of Fura-2 for Cd^{2+} (K_D 1×10^{-6} μM) markedly higher than that for Ca^{2+} (K_D 0.14 μM), Cd^{2+} retention within cells could be artifactual. Nevertheless, the results obtained using purified PMCA indicate that Cd^{2+} may prevent its own extrusion by impairing PMCA functionality. Supporting that results obtained using [^{125}I]TID-PC/16-labeled PMCA indicate that in the presence of Cd^{2+} the enzyme persisted in the E_2 conformation, becoming unable to start the reaction cycle. The sigmoidal inhibitory behavior of Cd^{2+} on the ATPase activity measured in the presence of Ca^{2+} may be explained in terms of two potential Cd^{2+} binding sites in PMCA with different affinities for the cation. Whereas the high-affinity Cd^{2+} binding site in PMCA contains a histidyl group, the low-affinity site contains a –SH group (Toledo-Maciel et al. 1998). Accordingly, the presence of 5 mM DTT did not abolish the inhibitory effect of Cd^{2+} on PMCA, since DTT will only prevent the binding of Cd^{2+} to the most superficial –SH groups, leaving the high-affinity binding site and/or the deeply buried –SH groups free to interact with the cation.

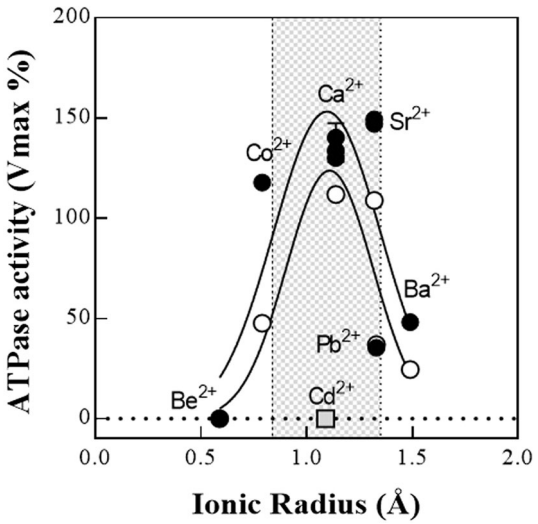

Fig. 11 DC-dependent PMCA ATPase activity relies on DCs ionic radii. Effect of DCs on PMCA ATPase activity measured in its auto-inhibited (*open circles*) or activated (*closed circles*) states (data taken from Table 2). Values of DC ion radii corresponding to their hexavalent coordination geometry were taken from http://www.webelements.com. *Gaussian curves* were adjusted to experimental data. *Shaded area* indicates the optimal range of DCs ionic radii for PMCA function. The value corresponding to Cd^{2+} (*shaded squares*) was not included in *curve* fitting

Moreover, another factor explains the inhibitory effect of Cd^{2+} on PMCA functionality: the modulation by Cd^{2+}-CaM. CaM is capable of binding other DCs besides Ca^{2+}. In fact, it has been reported that Cd^{2+} binds to two of the four Ca^{2+}-binding sites in CaM, with K_D ~4.5 μM for both sites (Suzuki et al. 1985). Although Ca^{2+} and Cd^{2+} induced similar conformational changes in CaM, it may not be sufficient to overcome the inhibition of PMCA activity imposed by Cd^{2+}. The consequences of Cd^{2+}-mediated impairment of PMCA activity on tissue functionality are twofold. First, by inhibiting PCMA, Cd^{2+} prevents its own extrusion causing its progressive accumulation within cells and triggering per se pro-apoptotic signaling pathways. And second, the inhibition of PMCA leads to increased Ca^{2+} concentration in cytoplasm that, depending on the final concentration reached, results in cell death via apoptosis or even necrosis.

Sr^{2+} is a nonessential metal for higher organisms, and no toxic effects for humans have been reported yet. In fact, some Sr^{2+} chelates are used in medicine to prevent osteoporosis because they promote the production of osteoblasts and decrease bone resorption by osteoclasts (Marie 2005). The chemical properties of Sr^{2+} are close to those of Ca^{2+}, and therefore, both cations share transporters and could bind to the same proteins (Pors Nielsen 2004). The fact that Sr^{2+} is poorly absorbed in the intestines and is highly excreted through urine (Pors Nielsen 2004) prevents its accumulation in the body. The slightly larger ionic radius of Sr^{2+} respect to that of Ca^{2+} decreases its binding affinity for most ligands. Overall, Sr^{2+} will not displace Ca^{2+} from its binding sites unless its concentration exceeds largely that of Ca^{2+} (Shirran and Barran 2009). Current results indicate that Sr^{2+} can enter HEK293T cells, being this process carried out mostly by the SOCs, as evidenced from its partial inhibition by La^{3+}. However, the possibility that other transporters may participate in Sr^{2+} entry cannot be ruled out, and their identification was beyond the scope of this work. In accordance with its low cytotoxicity, Sr^{2+} exited cells with a rate that was slightly lower than that of Ca^{2+}. Since the affinities of Fura-2 for both DCs are within the same order of magnitude (K_D 0.14 vs. 0.76 μM for Ca^{2+} and Sr^{2+}, respectively), the differences in the efflux rates observed in HEK293T cells could not be ascribed to higher tendency of the probe to retain Sr^{2+} within cells. In its auto-inhibited state, purified PMCA extruded Sr^{2+} with kinetic parameters comparable to those of Ca^{2+}. However, the catalytic efficiency of CaM-activated PMCA was ~50% lower for Sr^{2+} than for Ca^{2+}, which can result in lower Sr^{2+} efflux. Despite of this, PMCA contributes to

limit Sr^{2+} accumulation within cells and helps to prevent its potential toxic effects.

The most frequent symptoms of Ba^{2+} toxicity in humans include cardiac instability, muscle weakness, hypertension and respiratory failure (Bhoelan et al. 2014). It has been proposed that its entry in excitable cells occurs via the voltage-dependent Ca^{2+} channels (Heldman et al. 1989), but the mechanisms of Ba^{2+} uptake in non-excitable cells have not been elucidated yet. In HEK293T cells, SOCs constitute the main route of Ba^{2+} entry, as evidenced from its total inhibition with La^{3+}. Ba^{2+} was almost completely retained within cells, indicated by the very low efflux rate assessed with the probe Fura-2. Again, since this probe has the same affinity for Ca^{2+} and Ba^{2+} (K_D 0.14 μM), the differences observed in the efflux rates of these DCs could not be ascribed to a lower dissociation of Fura-2-Ba^{2+} complex that would retain the DC within cells. So far, there are few reports about the potential routes of Ba^{2+} efflux. For example, using whole-cell electrophysiological measurements, Thomas (2009) reported that PMCA from snail neurons transports Ba^{2+} with a rate equivalent to 20% of that measured for Ca^{2+} transport. These cells predominantly express PMCA2, which is constitutively activated and transports Ca^{2+} with kinetic features similar to those of CaM- or acidic phospholipid-activated PMCA4 (Mangialavori et al. 2012). The non-activated form of purified PMCA transported Ba^{2+} with V_{max} ~20% of that measured for Ca^{2+}, and this value increased twofold upon PMCA activation by CaM. Under physiological conditions, PMCA would not transport Ba^{2+} due to its low intracellular concentration—below PMCA $K_{0.5}$ for Ba^{2+}—and the presence of Ca^{2+} as competitive inhibitor of its transport. Therefore, PMCA may not constitute a main route for Ba^{2+} efflux, and it would not contribute significantly to Ba^{2+} detoxification.

Pb^{2+} is a recognized neurotoxicant that causes major alterations in the development of the central nervous system leading to cognitive and behavioral perturbations (Sanders et al. 2009). Pb^{2+} enters the neurons through the Ca^{2+} channels, its entry being enhanced in cells with depleted intracellular Ca^{2+} stores (Kerper and Hinkle 1997). Supporting that, our results show that Pb^{2+} entry in HEK293T cells also occurs via SOCs, as it was fully prevented by La^{3+}. Once within cells, Pb^{2+} promotes the release of Ca^{2+} from the endoplasmic reticulum and interferes with Ca^{2+} transport and with Ca^{2+}-dependent signaling pathways (Sanders et al. 2009). In particular, the exposure of human erythrocytes to micromolar concentrations of Pb^{2+} increases Ca^{2+} uptake and inhibits its efflux via PMCA in time- and concentration-dependent manners (Quintanar-Escorza et al. 2010), with a half inhibitory concentration (IC_{50}) estimated in 6 μM (Mas-Oliva 1989). Like Ba^{2+}, Pb^{2+} exit from HEK293T cells was negligible and leads to its accumulation. In this case, the low rate of Pb^{2+} efflux detected could be the resultant of both, the high affinity of Fura-2 for Pb^{2+} (K_D 4.2×10^{-6} μM) and the inhibition of PMCA. Supporting the latter hypothesis, we found that even when purified PMCA functioned in the presence of low concentrations of Pb^{2+} (<20 μM), the maximal velocity achieved—regardless PMCA activation state—was only ~30% of that measured in the presence of Ca^{2+} and CaM. Gramigni et al. (2009) proposed that Pb^{2+} inhibits Na^+, K^+ATPase—another member of the P-ATPases family—by impeding the hydrolysis of the phosphoenzyme E_2P. In case of this mechanism being operative in the current experimental system, it could account for PMCA inhibition by Pb^{2+}. Altogether, current results suggest that PMCA would be an important counteracting mechanism to preserve cell integrity during the initial steps of Pb^{2+} intoxication, but only when the intracellular concentration of the cation lies in the nanomolar or low micromolar range. In nucleated cells, once the concentration of intracellular Pb^{2+} rises, not only PMCA but also SERCA will be inactivated (Hechtenberg and Beyersmann 1991). In erythrocytes, the lack of SERCA exacerbates the cytotoxic effects of Pb^{2+} by impeding Ca^{2+} and its own exit through PMCA, and triggering the signaling cascade that leads to eryptosis, a common feature in Pb^{2+}-exposed workers (Aguilar-Dorado et al. 2014).

The only transition metal included in this study, Co^{2+}, is a normal component of diverse coenzymes and metalloenzymes (Harrop and Mascharak 2013; Odaka and Kobayashi 2013). However, its excessive accumulation is cytotoxic and ultimately leads to cell death (Simonsen et al. 2012). In erythrocytes, the uptake of Co^{2+} shares some similarities with Ca^{2+} entry. Using $^{57}Co^{2+}$ and $^{45}Ca^{2+}$, it has been demonstrated that both cations compete for common channel-like and carrier-mediated uptake pathways (Simonsen et al. 2011b). However, Co^{2+} uptake in HEK293T occurred through a transporter(s) different from SOCs, as its entry was not prevented by La^{3+}. The identification of the transporter(s) that participate in Co^{2+} uptake by these cells was beyond the scope of this work and requires further investigation. To the best of our knowledge, the mechanism of Co^{2+} exit from cells has not been described yet. Results obtained in HEK293T cells are not conclusive, but suggest that PMCA could partially contribute to eliminate excessive intracellular Co^{2+}. Supporting this hypothesis, and even though in the absence of activators the maximal velocity of Co^{2+} transport was only ~50% of that measured for Ca^{2+}, this value raised to ~90% in CaM-activated PMCA. Like Ca^{2+}, Co^{2+} modified CaM conformation, although the concentration of Co^{2+} necessary to achieve the maximal effect was four times higher than that of Ca^{2+}. In the particular case of erythrocytes, even when Co^{2+} can be extruded via PMCA, its strong binding to hemoglobin will limit the concentration of free cation available to be transported (Simonsen et al. 2011a). Thus, it cannot be ruled out the possibility that this DC

may remain attached to negatively charged molecules in nucleated cells which would prevent Co^{2+} efflux and lead to its progressive accumulation.

Be^{2+} is the lightest DC of this group, with some chemical properties that resemble those of aluminum (Al^{3+}) (Habashi 2013). Human exposure to this DC causes diverse pathologies, including contact allergy, pneumonitis and, upon prolonged exposure, berylliosis—a granulomatous lung disease—and cancer (Uversky 2013). Due to its similarities with Mg^{2+}, Be^{2+} displaces it from its binding sites in certain proteins and affects their biological functions (Emsley 2001). The mechanisms underlying cell uptake of Be^{2+} are still not elucidated, but we observed that SOCs would not mediate its transport in HEK293T cells, as Be^{2+} uptake was minimal and not inhibited by La^{3+}. Nevertheless, a slow but sustained efflux of this cation was evidenced in these cells. The finding that purified PMCA did not transport this DC—not even when in its fully activated state—and that no Be^{2+}-associated PMCA ATPase activity was detected, allowed us to discard the possibility that PMCA would mediate the extrusion of Be^{2+} from HEK293T cells. On the contrary, Be^{2+} may inhibit PMCA by replacing its cofactor (Mg^{2+}) from its binding site. Therefore, Be^{2+} exit from cells must proceed by one or more PMCA-independent mechanisms, and further investigation is required to determine the channels/transporters involved in this process.

In summary, our findings indicate that, in addition to Ca^{2+}, PMCA transports Sr^{2+} both in vitro and in cultured cells, and with kinetic parameters close to those of Ca^{2+}. Regarding Co^{2+} and Pb^{2+}, these cations increased PMCA ATPase activity and induced a proper conformational change in the pump. However, they were poorly transported, making these cations partial uncouplers of PMCA transport activity. Results obtained in intact cells suggest that PMCA could partially contribute to their efflux, even when the possibility of passive DC leak could not be discarded. Finally, Cd^{2+}, Ba^{2+} and Be^{2+} were not transported by PMCA. These findings have profound implications on the toxicological effects of the DCs investigated. Under physiological conditions, the concentration of free Ca^{2+} in the cytoplasm is ~100 nM, and PMCA will be auto-inhibited but still able to transport the DCs. Hence, the efflux of certain DCs via PMCA will limit their accumulation in the cells and partially prevent their toxic effects. In contrast, the irreversible inactivation of PMCA by Cd^{2+} will not only contribute to its own accumulation in the cells, but also of Ca^{2+} that will trigger intracellular signals that lead to cell death.

Acknowledgements This work was supported by grants of Agencia Nacional de Promoción Científica y Tecnológica (ANPCyT), Consejo Nacional de Investigaciones Científicas y Técnicas (CONICET) and Secretaria de Ciencia y Técnica de la Universidad de Buenos Aires (UBACyT), Argentina. Authors are grateful to Dr. Osvaldo Rey for the generous gift of HEK293T cells.

Compliance with ethical standards

Conflict of interest The authors declare that they have no conflict of interest.

References

Aguilar-Dorado IC, Hernandez G, Quintanar-Escorza MA, Maldonado-Vega M, Rosas-Flores M, Calderon-Salinas JV (2014) Eryptosis in lead-exposed workers. Toxicol Appl Pharmacol 281(2):195–202

Akatsu H, Hori A, Yamamoto T et al (2012) Transition metal abnormalities in progressive dementias. Biometals 25(2):337–350

Bhoelan BS, Stevering CH, van der Boog AT, van der Heyden MA (2014) Barium toxicity and the role of the potassium inward rectifier current. Clin Toxicol (Phila) 52(6):584–593

Bouron A, Altafaj X, Boisseau S, De Waard M (2005) A store-operated Ca2+ influx activated in response to the depletion of thapsigargin-sensitive Ca2+ stores is developmentally regulated in embryonic cortical neurons from mice. Brain Res Dev Brain Res 159(1):64–71

Breuer W, Epsztejn S, Millgram P, Cabantchik IZ (1995) Transport of iron and other transition metals into cells as revealed by a fluorescent probe. Am J Physiol 268(6 Pt 1):C1354–C1361

Brooks SP, Storey KB (1992) Bound and determined: a computer program for making buffers of defined ion concentrations. Anal Biochem 201(1):119–126

Chao SH, Suzuki Y, Zysk JR, Cheung WY (1984) Activation of calmodulin by various metal cations as a function of ionic radius. Mol Pharmacol 26(1):75–82

Emsley J (2001) Nature's building blocks: an A-Z guide to the elements. Oxford University Press, Oxford

Ferreira-Gomes MS, Gonzalez-Lebrero RM, de la Fuente MC, Strehler EE, Rossi RC, Rossi JP (2011) Calcium occlusion in plasma membrane Ca2+-ATPase. J Biol Chem 286(37):32018–32025

Filoteo AG, Enyedi A, Penniston JT (1992) The lipid-binding peptide from the plasma membrane Ca2+ pump binds calmodulin, and the primary calmodulin-binding domain interacts with lipid. J Biol Chem 267(17):11800–11805

Fiske CH, Subbarow Y (1925) The colorimetric determination of phosphorus. J Biol Chem 66(2):375–400

Gramigni E, Tadini-Buoninsegni F, Bartolommei G, Santini G, Chelazzi G, Moncelli MR (2009) Inhibitory effect of Pb2+ on the transport cycle of the Na+, K+-ATPase. Chem Res Toxicol 22(10):1699–1704

Habashi F (2013) Beryllium, physical and chemical properties. In: Kretsinger RH, Uversky VN, Permyakov EA (eds) Encyclopedia of metalloproteins. Springer, New York, pp 255–257

Harrop TC, Mascharak PK (2013) Cobalt-containing enzymes. In: Kretsinger RH, Uversky VN, Permyakov EA (eds) Encyclopedia of metalloproteins. Springer, New York, pp 684–690

Hechtenberg S, Beyersmann D (1991) Inhibition of sarcoplasmic reticulum Ca(2+)-ATPase activity by cadmium, lead and mercury. Enzyme 45(3):109–115

Heldman E, Levine M, Raveh L, Pollard HB (1989) Barium ions enter chromaffin cells via voltage-dependent calcium channels and induce secretion by a mechanism independent of calcium. J Biol Chem 264(14):7914–7920

James P, Vorherr T, Krebs J et al (1989) Modulation of erythrocyte Ca2+-ATPase by selective calpain cleavage of the calmodulin-binding domain. J Biol Chem 264(14):8289–8296

Jarup L, Akesson A (2009) Current status of cadmium as an environmental health problem. Toxicol Appl Pharmacol 238(3):201–208

Kerper LE, Hinkle PM (1997) Cellular uptake of lead is activated by depletion of intracellular calcium stores. J Biol Chem 272(13):8346–8352

Kwan CY, Putney JW Jr (1990) Uptake and intracellular sequestration of divalent cations in resting and methacholine-stimulated mouse lacrimal acinar cells. Dissociation by Sr2+ and Ba2+ of agonist-stimulated divalent cation entry from the refilling of the agonist-sensitive intracellular pool. J Biol Chem 265(2):678–684

Liu C-Y, Lee NM, Wang T-H (1997) Chelation ion chromatography as a technique for trace elemental analysis in complex matrix samples. Anal Chim Acta 337(2):173–182

Lopreiato R, Giacomello M, Carafoli E (2014) The plasma membrane calcium pump: new ways to look at an old enzyme. J Biol Chem 289(15):10261–10268

Mangialavori I, Villamil Giraldo AM, Marino Buslje C, Ferreira Gomes M, Caride AJ, Rossi JP (2009) A new conformation in sarcoplasmic reticulum calcium pump and plasma membrane Ca2+ pumps revealed by a photoactivatable phospholipidic probe. J Biol Chem 284(8):4823–4828

Mangialavori I, Ferreira-Gomes M, Pignataro MF, Strehler EE, Rossi JP (2010) Determination of the dissociation constants for Ca2+ and calmodulin from the plasma membrane Ca2+ pump by a lipid probe that senses membrane domain changes. J Biol Chem 285(1):123–130

Mangialavori IC, Corradi G, Rinaldi DE, de la Fuente MC, Adamo HP, Rossi JP (2012) Autoinhibition mechanism of the plasma membrane calcium pump isoforms 2 and 4 studied through lipid–protein interaction. Biochem J 443(1):125–131

Marie PJ (2005) Strontium ranelate: a novel mode of action optimizing bone formation and resorption. Osteoporos Int 16(Suppl 1):S7–S10

Mas-Oliva J (1989) Effect of lead on the erythrocyte (Ca2+, Mg2+)-ATPase activity calmodulin involvement. Mol Cell Biochem 89(1):87–93

Niggli V, Penniston JT, Carafoli E (1979) Purification of the (Ca2+-Mg2+)-ATPase from human erythrocyte membranes using a calmodulin affinity column. J Biol Chem 254(20):9955–9958

Odaka M, Kobayashi M (2013) Cobalt proteins, overview. In: Kretsinger RH, Uversky VN, Permyakov EA (eds) Encyclopedia of metalloproteins. Springer, New York, pp 670–678

Panayi AE, Spyrou NM, Iversen BS, White MA, Part P (2002) Determination of cadmium and zinc in Alzheimer's brain tissue using inductively coupled plasma mass spectrometry. J Neurol Sci 195(1):1–10

Pfleger H, Wolf HU (1975) Activation of membrane-bound high-affinity calcium ion-sensitive adenosine triphosphatase of human erythrocytes by bivalent metal ions. Biochem J 147(2):359–361

Pors Nielsen S (2004) The biological role of strontium. Bone 35(3):583–588

Quintanar-Escorza MA, Gonzalez-Martinez MT, del Pilar IO, Calderon-Salinas JV (2010) Oxidative damage increases intracellular free calcium [Ca^{2+}]i concentration in human erythrocytes incubated with lead. Toxicol In Vitro 24(5):1338–1346

Rega AF, Garrahan PJ (1986) The Ca^{2+} pump of plasma membranes. CRC Press, Boca Raton

Rossi JP, Schatzmann HJ (1982) Is the red cell calcium pump electrogenic? J Physiol 327:1–15

Sanders T, Liu Y, Buchner V, Tchounwou PB (2009) Neurotoxic effects and biomarkers of lead exposure: a review. Rev Environ Health 24(1):15–45

Shirran SL, Barran PE (2009) The use of ESI–MS to probe the binding of divalent cations to calmodulin. J Am Soc Mass Spectrom 20(6):1159–1171

Silbergeld EK (1992) Mechanisms of lead neurotoxicity, or looking beyond the lamppost. FASEB J 6(13):3201–3206

Simons TJ (1993) Lead–calcium interactions in cellular lead toxicity. Neurotoxicology 14(2–3):77–85

Simonsen LO, Brown AM, Harbak H, Kristensen BI, Bennekou P (2011a) Cobalt uptake and binding in human red blood cells. Blood Cells Mol Dis 46(4):266–276

Simonsen LO, Harbak H, Bennekou P (2011b) Passive transport pathways for Ca(2+) and Co(2+) in human red blood cells. (57)Co(2+) as a tracer for Ca(2+) influx. Blood Cells Mol Dis 47(4):214–225

Simonsen LO, Harbak H, Bennekou P (2012) Cobalt metabolism and toxicology—a brief update. Sci Total Environ 432:210–215

Steck TL, Weinstein RS, Straus JH, Wallach DF (1970) Inside-out red cell membrane vesicles: preparation and purification. Science 168(3928):255–257

Strehler EE, Zacharias DA (2001) Role of alternative splicing in generating isoform diversity among plasma membrane calcium pumps. Physiol Rev 81(1):21–50

Sumida M, Hamada M, Takenaka H, Hirata Y, Nishigauchi K, Okuda H (1986) Ca2+, Mg2+-ATPase of microsomal membranes from bovine aortic smooth muscle: effects of Sr2+ and Cd2+ on Ca2+ uptake and formation of the phosphorylated intermediate of the Ca2+, Mg2+-ATPase. J Biochem 100(3):765–772

Suzuki Y, Chao SH, Zysk JR, Cheung WY (1985) Stimulation of calmodulin by cadmium ion. Arch Toxicol 57(3):205–211

Thastrup O, Dawson AP, Scharff O et al (1989) Thapsigargin, a novel molecular probe for studying intracellular calcium release and storage. Agents Actions 27(1–2):17–23

Thevenod F (2010) Catch me if you can! Novel aspects of cadmium transport in mammalian cells. Biometals 23(5):857–875

Thevenod F, Lee WK (2013) Cadmium and cellular signaling cascades: interactions between cell death and survival pathways. Arch Toxicol 87(10):1743–1786

Thomas RC (2009) The plasma membrane calcium ATPase (PMCA) of neurones is electroneutral and exchanges 2 H^+ for each Ca^{2+} or Ba^{2+} ion extruded. J Physiol 587(2):315–327

Toledo-Maciel A, Goncalves-Gomes S, de Gouveia Castex M, Vieyra A (1998) Progressive inactivation of plasma membrane ($Ca^{2++}Mg^{2+}$)ATPase by Cd^{2+} in the absence of ATP and reversible inhibition during catalysis. Biochemistry 37(44):15261–15265

Uversky VN (2013) Beryllium as antigen. In: Kretsinger RH, Uversky VN, Permyakov EA (eds) Encyclopedia of metalloproteins. Springer, New York, pp 251–255

Vats YA, Fedirko NV, Klevets MY, Voitenko NV (2002) Role of SH groups in the functioning of Ca^{2+}-transporting ATPases regulating Ca2+ homeostasis and exocytosis. Neurophysiology 34(1):5–12

Verbost PM, Flik G, Pang PK, Lock RA, Wendelaar Bonga SE (1989) Cadmium inhibition of the erythrocyte Ca2+ pump. A molecular interpretation. J Biol Chem 264(10):5613–5615

Verstraeten SV (2014) Participation of reactive oxygen species in the toxicity of cobalt, nickel, cadmium and mercury. In: Catalá A (ed) Reactive oxygen species, lipid peroxidation and protein oxidation. Nova Science Publishers Inc., New York, pp 95–126

Yuan Y, Jiang CY, Xu H et al (2013) Cadmium-induced apoptosis in primary rat cerebral cortical neurons culture is mediated by a calcium signaling pathway. PLoS One 8(5):e64330